View metadata, citation and similar papers at core.ac.uk

brought to you by CORE

provided by Open Archive Toulouse Archive Ouverte

Open Archive Toulouse Archive Ouverte (OATAO)

OATAO is an open access repository that collects the work of Toulouse researchers and makes it freely available over the web where possible.

This is an author-deposited version published in: http://oatao.univ-toulouse.fr/
Eprints ID: 10381

DOI:10.1039/b505654c
Official URL: http://dx.doi.org/10.1039/b505654c

To cite this version:
Cordier, Anne and Flahaut, Emmanuel and Viazzi, Céline and Laurent, Christophe and Peigney, Alain *In situ CCVD synthesis of carbon nanotubes within a commercial ceramic foam.* (2005) Journal of Materials Chemistry, vol. 15 (n° 37). pp. 4041-4050. ISSN 0959-9428

Any correspondence concerning this service should be sent to the repository administrator:
staff-oatao@inp-toulouse.fr

In situ CCVD synthesis of carbon nanotubes within a commercial ceramic foam

Anne Cordier, Emmanuel Flahaut, Céline Viazzi, Christophe Laurent and Alain Peigney*

DOI: 10.1039/b505654c

Consolidated nanocomposite foams containing a large quantity of carbon nanotubes (CNTs) within millimetre-sized pores are prepared for the first time. A commercial ceramic foam is impregnated by a 60 g L^{-1} slurry of a $(Mg_{(1-x)}(Co_{0.75}Mo_{0.25})_xO$ solid solution (x = 0.01, 0.05, 0.1 and 0.2) powder in ethanol. Three successive impregnations led to deposits several tens of μm thick, with a good coverage of the commercial-ceramic pore walls but without closing the pores. The materials were submitted to a CCVD treatment in H_2–CH_4 atmosphere in order to synthesise the CNTs. When using attrition-milled powders, the carbon is mostly in the form of nanofibres or disordered carbon rather than CNTs. Using non-milled powders produces a less-compact deposit of catalytic material with a higher adherence to the walls of the ceramic foam. After CCVD, the carbon is mostly in the form of high-quality CNTs, as when using powder beds, their quantity being 2.5 times higher. The so-obtained consolidated nanocomposite materials show a multi-scale pore structuration.

1.0 Introduction

Because of new environmental regulations, much research is focused on materials that are intended to decrease the atmospheric pollution created by human activity. Novel or improved materials for heterogeneous catalysis are of primary importance. Such materials are generally made of a substrate on which a large quantity of nanometre-sized active particles are dispersed and stabilised. Ceramic foams are attractive as substrates because they offer a lower pressure drop, high geometric surface areas and greater turbulence than packed beds.[1,2] However, the sintering of such materials, necessary to improve their mechanical properties, is detrimental to their surface area. To solve this problem, the preparation of materials in which the pore walls are covered by a ceramic layer made of submicronic grains, generally γ-Al_2O_3, has been reported by several authors.[3,4] The use of filamentous carbon was also reported[5] in order to obtain higher surface areas and to ensure a better heat transfer. Besides their outstanding mechanical[6] and electrical[7] properties, carbon nanotubes (CNTs) display a very high thermal conductivity in the longitudinal direction[6] and a very high specific surface area,[8] close to 1315 m^2 g^{-1} for single-walled CNTs (SWNTs). CNTs thus appeared very attractive as nanometric catalytic particle substrates for heterogeneous catalysis.[9–14] Consequently, the preparation of a novel composite catalyst substrate, combining a ceramic foam and CNTs for a highly accessible surface area and a good heat transfer, is a major issue.

The present group reported earlier the synthesis of CNT–metal–oxide nanocomposite powders by the selective reduction in a H_2–CH_4 atmosphere of different oxide solid solutions.[15–17] Metallic nanoparticles formed *in situ* at about 1000 °C have a size adequate for the formation of CNTs from the catalytic decomposition of CH_4. Rul *et al.*[18] have prepared CNT–metal–ceramic foams by selective reduction of $Mg_{0.9}Co_{0.1}Al_2O_4$ solid solution foams, as opposed to powders, which were prepared beforehand by the gelcasting foam method. Despite the high quality of the obtained CNTs, these materials were not suitable as catalyst substrates because of their fairly poor mechanical properties. Similar results were obtained through the impregnation of commercial poly(urethane) foams with the solid solution.[19] In order to overcome this difficulty, a commercial consolidated ceramic foam is used in the present study. This material is impregnated by a slurry of MgO-based solid solution, which constitutes the catalytic material used for the formation of CNTs. The aim is to tailor the so-obtained material in order to ensure that the CNTs formed upon reduction do homogeneously fill the open porosity of the ceramic foam. The preparation conditions to optimise the impregnation of the commercial ceramic foam were studied in order to obtain a material containing the maximum quantity of CNTs. The influence of the concentration of the slurry, the number of impregnations, attrition-milling (or not) of the starting powder and the quantity of catalytic material are investigated. The quantity and quality of the CNTs are compared with data obtained using a powder bed as starting material.

2.0 Experimental procedures

2.1 Preparation

The different steps of the preparation method (Fig. 1) are briefly outlined here. Powders of the oxide solid solutions (catalytic material) were prepared by the combustion route. Slurries were prepared with the different powders, in a process that either includes or does not include an attrition-milling

CIRIMAT, UMR CNRS-UPS-INP 5085, Bat. 2R1, Université Paul-Sabatier, 31062 Toulouse cedex 4, France. E-mail: peigney@chimie.ups-tlse.fr; Fax: +33 (0)5 61 55 61 63; Tel: +33 (0)5 61 55 61 75

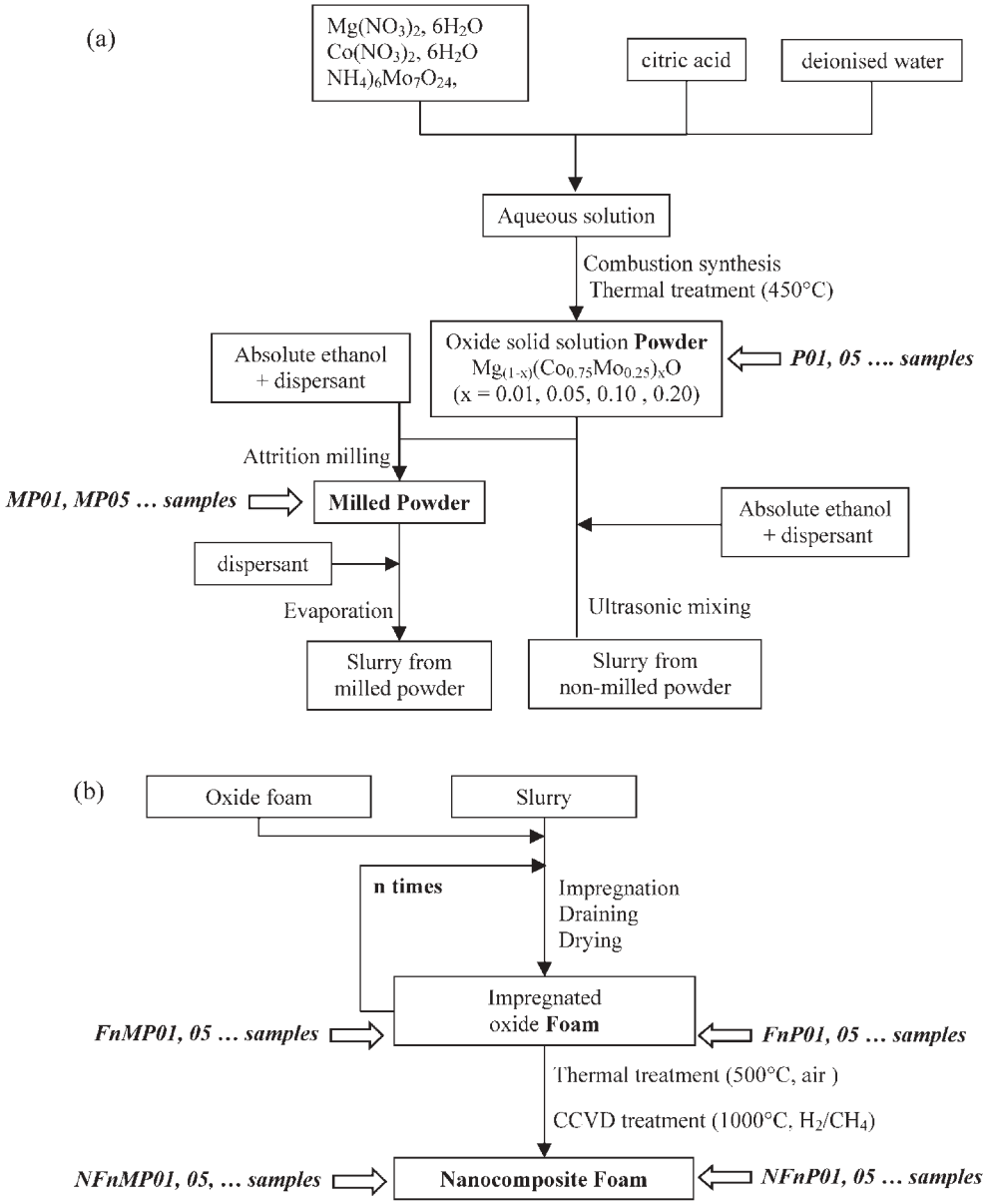

Fig. 1 Flow-charts of slurry preparation (a) and of the CNT-containing nanocomposite foams preparation (b). The preparation of nanocomposite powder beds was omitted from (b) for clarity.

step. Then, commercial consolidated ceramic foams were impregnated by the slurries. After drying and thermal treatment at a moderate temperature, a stable film of catalytic material was obtained on the walls of the ceramic foam. Finally, this impregnated foam was submitted to the CCVD treatment for the formation of CNTs.

2.1.1 Synthesis of the oxide solid solution. The starting powders were synthesised by the combustion route.[20,21] The formula of the desired combustion products[22] is written as $Mg_{(1-x)}(Co_{0.75}Mo_{0.25})_xO$ (x = 0.01, 0.05, 0.1 and 0.2), although these oxides are definitely not solid solutions because the molybdenum ions do not enter the rock-salt lattice of MgO. The combustion process was described in a previous work.[22] $Mg(NO_3)_2{\cdot}6H_2O$ and $Co(NO_3)_2{\cdot}6H_2O$ were dissolved in deionised water together with the required amount of $(NH_4)_6Mo_7O_{24}{\cdot}4H_2O$ as well as citric acid. Citric acid was used as the fuel in the combustion process, using the so-called stoichiometric ratio.[20] The Pyrex dish containing the solution was placed in a furnace preheated at 550 °C. The solution immediately started to boil and dehydrate. The resulting paste frothed and then blazed. No flame occurred and a rather light material was produced which swelled to the capacity of the Pyrex dish. The total combustion process was over in less than 10 min. The combustion product was calcined in air (450 °C, 1 h) to remove carbon residues (Fig. 1a). These powders are named P01, P05, P10 and P20, for x values equal to 0.01, 0.05, 0.10 and 0.20, respectively. For the sake of comparison, a pure MgO powder was synthesised by the same route.

2.1.2. Attrition-milling and slurry preparation. The above P powders were mixed with a dispersant (BEYCOSTAT C213,

CECA France, 1 mg m^{-2} of powder) in absolute ethanol using ultrasonic agitation for 10 min (Fig. 1a). Then, the slurry was kept under magnetic stirring to prevent sedimentation. Absolute ethanol was used to prevent the dissolution of the MgO-based oxides and the subsequent formation of $Mg(OH)_2$ which would immediately precipitate and lead to a very viscous medium. In some cases, the powder was attrition-milled (2000 rpm, 30 min) in the dispersant–absolute ethanol medium, using a Nylon vessel and rotor and α-alumina balls (200–300 μm in diameter). The ratio between the powder volume and the volume of the balls was 0.5. After attrition-milling, the alumina balls were separated by rinsing in absolute ethanol and filtering. The final volume was adjusted by partial evaporation, producing a slurry prepared from milled powders (MP). These MP samples are named MP01, MP05, MP10 and MP20, for x values equal to 0.01, 0.05, 0.10 and 0.20, respectively (Fig. 1a). Note that the MP samples were dried only for the measure of the specific surface area.

2.1.3 Impregnation of commercial ceramic foam. The commercial ceramic foams (Aluminium Martigny France) are composed mainly of α-alumina (more than 85 wt%) with some mullite and cristobalite. Their shape is cylindrical (diameter 32 mm; height 22 mm, Fig. 2a). The porosity is equal to 50 pores per inch (ppi), with a pore diameter in the range 0.5–1.5 mm (Fig. 2b). The ceramic grains are not larger than 10 μm and some porosity remains within the ceramic walls (Fig. 2c). The ceramic foam was soaked into the slurry, drained and dried in air. Several successive impregnations were necessary to obtain a homogeneous deposit and to prevent the obstruction of the pores (Fig. 1b). The foam was dried in air (3h) between two successive impregnations. The impregnated foam was then calcined in flowing air (500 °C, heating rate 50 °C.h^{-1}) to remove ethanol, dispersant and possible Nylon residues (for MP samples) (Fig. 1b). These impregnated foams are named FnP01, FnP05–20 and FnMP01, FnMP05–20, with n as the number of impregnations used in the process.

2.1.4. Synthesis of carbon nanotubes. The impregnated foams were reduced (Fig. 1b) in a H_2–CH_4 gas mixture[17] (20 mol.% CH_4, heating and cooling rates 5 °C min^{-1}, maximum temperature 1000 °C, no dwell). The selective reduction of the starting oxide leads to the formation of nanometric metal particles which immediately catalyse the decomposition of CH_4 and the subsequent formation of a single CNT on each active metal particle. This resulted in a CNT-containing composite foam with a very homogeneous dispersion of the CNTs around the grains of the oxide catalytic material. The nanocomposite foam (NF) series are named NFnP01, NFnP05—20 and NFnMP01, NFnMP05–20 (Fig. 1b). For the sake of comparison, some powder beds were also reduced, giving rise to the NP series (for the sake of clarity, this was not mentioned in Fig. 1b).

2.2 Characterisation

The oxide solid solution powders were characterised by X-ray diffraction (XRD, Bruker D4 ENDEAVOR). The specific surface area of the catalytic materials and impregnated ceramic foams was measured by the BET method (Micrometrics Flow Sorb II 2300) using N_2 adsorption at liquid N_2 temperature. The carbon content in the nanocomposite foams (C_n (wt%)) was measured by the flash combustion method. The starting commercial ceramic foams and the impregnated foams were observed by scanning electron microscopy (SEM, JEOL JSM 35CF) in order to evaluate the deposit quality. The nanocomposite foams (NF) were observed by field-emission-gun SEM (FEG-SEM, JEOL JSM 6700F service commun TEMSCAN, UFR, PCA of Université Paul Sabatier) in order to

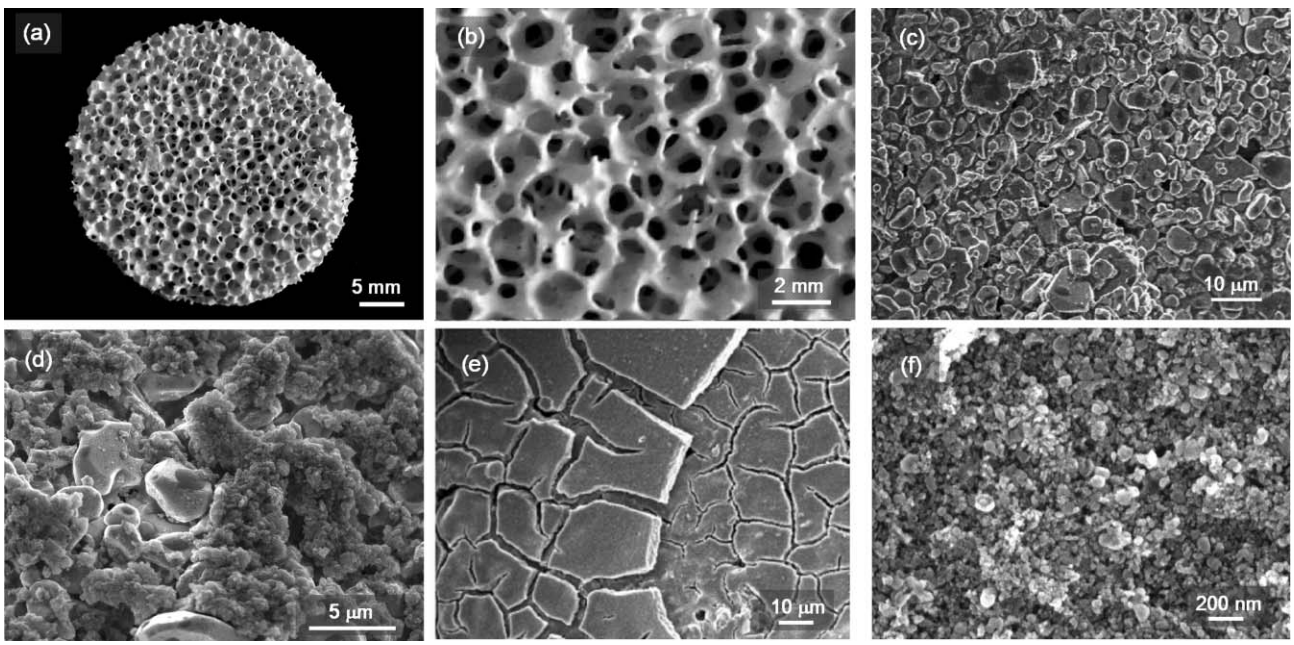

Fig. 2 SEM images of the commercial ceramic foam (a–c) and of the deposit of catalytic material after three impregnations using a slurry at a powder concentration of 40 g L^{-1} (d) and 60 g L^{-1} (e–f).

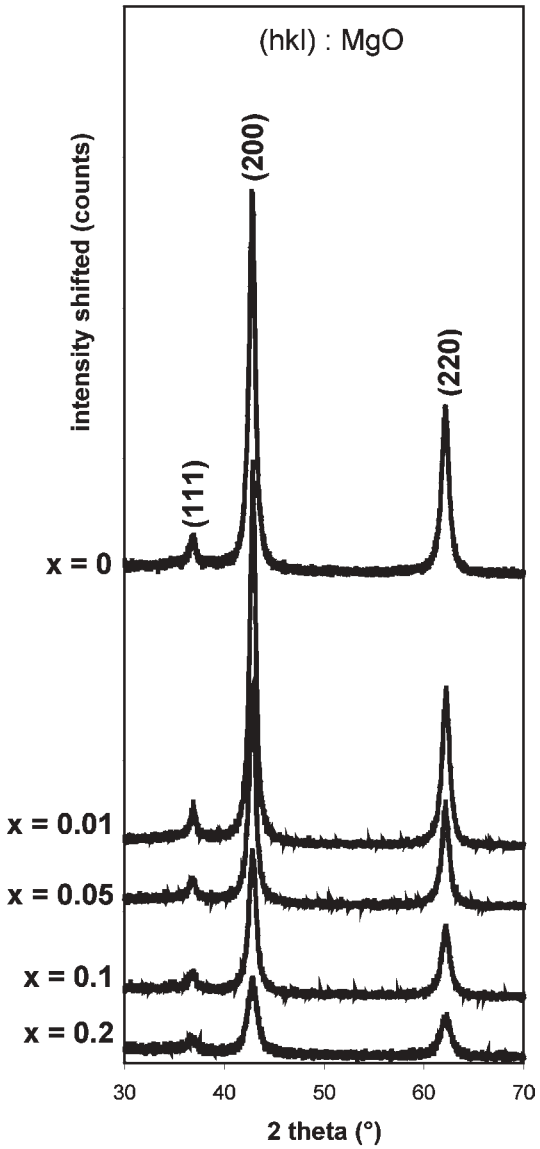

Fig. 3 XRD patterns of oxide solid solution powders $Mg_{(1-x)}(Co_{0.75}Mo_{0.25})_xO$.

discriminate the presence of CNTs and carbon nanofibres and to evaluate the quantity of CNTs in the NF. The CNTs were characterised by Raman spectroscopy (Jobin–Yvon Labram spectrometer using a 514.5 nm Ar^+ laser, run in back-scattered confocal arrangement). The intensity ratio between the D and G bands ($I_{D/G}$) was calculated to compare the proportions of carbon in sp^3 configuration in the different specimens.

3.0 Results and discussions

3.1 Powders of oxide solid solutions

Only the main diffraction peaks of the MgO rock-salt type structure are detected on the XRD patterns of the pure MgO and P01, P05, P10 and P20 powders (Fig. 3). Their intensity regularly decreases when x increases. The crystallite size, calculated from the peak width at half-maximum using the Scherrer formula, does not show a significant decrease, from 11.1 ± 1.1 nm for pure MgO (x = 0) to 8.4 ± 0.8 nm for P20 (x = 0.2). However, from pure MgO to P20, 70 and 63% decreases were measured in the (200) and (220) peak areas, respectively, which clearly indicate a significant loss of crystallinity. No minor-phase peaks were detected, particularly no peak which would correspond to Co_3O_4. Thus, we infer that the cobalt ions are substituting for Mg^{2+} ions in the cationic sub-lattice of MgO. Consequently, increasing the cobalt substitution rate appears to mainly decrease the crystallisation degree with only a minor effect on the crystallite size. However, because of the poor crystallisation state of the powders, the uncertainties on the cell parameters were too high to detect a significant evolution versus x. No molybdenum oxide was detected. However, a previous work[23] has shown that in similar products synthesised by ureic combustion, with a much higher crystallisation degree than the present powders synthesised by citric acid combustion, molybdenum ions were not substituted to Mg^{2+} in the cationic sub-lattice of MgO and were therefore assumed to be in the form of an oxide of ill-defined composition MoO_y. The specific surface area of the P powders ($(S_{ss})_P$, Table 1) is about 90 ± 10 $m^2\ g^{-1}$. There was a notable increase in specific surface area, in the range 125–185 $m^2\ g^{-1}$ ($(S_{ss})_{MP}$, Table 1), after attrition-milling.

Table 1 Some characteristics of the attrition-milled oxide powders (MP samples), the oxide foams prepared using slurries (3 impregnations; 60 g L^{-1}) made with attrition-milled powders (F3MP samples) and the corresponding nanocomposite foams (NF3MP samples) obtained after the CCVD treatment. All data are reported versus x (x = 0.01, 0.05, 0.1 and 0.2) in the starting oxide solid solution $Mg_{(1-x)}(Co_{0.75}Mo_{0.25})_xO$. For the sake of comparison, data for the corresponding non-milled oxide powders (P samples) and nanocomposite powders (NP samples) are also included

x		0.01	0.05	0.10	0.20
MP	$(S_{ss})_{MP}/m^2\ g^{-1}$ [a]	126 ± 13	187 ± 19	184 ± 18	153 ± 15
F3MP	m_{CM} (wt%) [b]	5.94 ± 0.57	4.82 ± 0.45	7.77 ± 0.53	6.41 ± 0.45
NF3MP	C_n (wt%) [c]	1.18 ± 0.12	3.99 ± 0.40	5.25 ± 0.53	8.45 ± 0.85
	$(C_n)_{CM}$ [d](wt%)	19.9 ± 3.6	82.8 ± 9.8	67.6 ± 6.0	132 ± 11
P	$(S_{ss})_P/m^2\ g^{-1}$ [e]	80.7 ± 2.4	94.6 ± 2.8	102 ± 3.1	100 ± 3.0
NP	$(C_n)_P$ (wt%) [f]	16.1 ± 0.3	27.4 ± 0.5	38.6 ± 0.8	35.5 ± 0.7
Foam/powder bed comparison	$(C_n)_{CM}$ / $(C_n)_P$	1.2	3	1.7	3.7

[a] $(S_{ss})_{MP}$: specific surface area of the attrition-milled oxide powders. [b] m_{CM}: mass of the corresponding catalytic material (wt%) impregnated in the commercial foam. [c] C_n: carbon content (wt%) in the nanocomposite foam after the CCVD treatment, relative to the mass of the nanocomposite foam. [d] $(C_n)_{CM}$: carbon content (wt%) in the nanocomposite foam after the CCVD treatment, relative to the mass of catalytic material impregnated in the foam. [e] $(S_{ss})_P$: specific surface area of the corresponding non-milled oxide powders. [f] $(C_n)_P$: carbon content (wt%) in the corresponding nanocomposite powder bed.

3.2 Foams impregnated with attrition-milled powders

3.2.1 Oxide foams (F*n*MP specimens). The influence of the powder concentration in the slurry (40 or 60 g L^{-1}) was studied using the MP01 powder. Concentrations higher than 60 g L^{-1} produced slurries too viscous to be suitable for the process. Three successive impregnations were performed with each slurry. For the 40 g L^{-1} slurry, SEM observations (Fig. 2d) revealed large areas without any deposit of catalytic material, which could indicate that the concentration is too low to produce a homogeneous deposit. A much more homogeneous deposit was observed for the 60 g L^{-1} slurry. The thickness is not higher than 10 μm for each deposited layer and many cracks are observed, formed during the (probably too-fast) drying of the material (Fig. 2e). The microstructure of the oxide deposit is revealed at a higher magnification (Fig. 2f). It consists of grains smaller than 100 nm with pores whose diameters are not larger that a few tens of nanometers. We thus chose to use 60 g L^{-1} slurries for all other preparations in the following.

The influence of the number of impregnations (n, Fig. 1b) was studied using a slurry prepared with the MP01 powder. Both the weight of catalytic material impregnated (m_{CM}, Table 1) and the specific surface area of the impregnated foam (S_{IF}), measured after the 500 °C calcination, were followed versus n. Each S_{IF} datum is an average value calculated from the specific surface area of three samples. There is a linear increase of m_{CM} with n (Table 1 and Fig. 4a). S_{IF} sharply increases up to $n = 3$ but tends to be almost constant for higher n values (Fig. 4b). It seems that the deposit becomes more compact for more than three impregnations. The smallest porosity of the first layers probably becomes inaccessible or closed. In addition, the deposit becomes less adherent to the ceramic foam walls for $n = 4$ and 5. For these reasons, all the other experiments in the following were performed with three successive impregnations ($n = 3$).

3.2.2 Nanocomposite foams (NF3MP specimens). The ceramic foams impregnated in the conditions determined above were selectively reduced by CCVD treatment. Some characteristics of the materials versus x (x = 0.01, 0.05, 0.1 and 0.2) in the starting oxide solid solution $Mg_{(1-x)}(Co_{0.75}Mo_{0.25})_xO$ are reported in Table 1. Although x is the main variable between the four samples, it is worth noting that both the specific surface area of the milled powders $(S_{ss})_{MP}$ and the weight of impregnated catalytic material (m_{CM}) also vary somewhat from one specimen to another. The carbon content in the composite foam (C_n) regularly increases from 1.18 to 8.45 wt% when x is increased from 0.01 to 0.20 (Table 1). Thus, the variation of C_n is clearly correlated with that of x, which is the key variable, and it was considered that the variations of $(S_{ss})_{MP}$ and m_{CM} have only a minor influence. Indeed, the quantity of metal obtained upon reduction increases with x, which usually also corresponds to an increase in the quantity of catalytic metal nanoparticles and, consequently, also in more deposited carbon. C_n was divided by the weight of impregnated catalytic material (m_{CM}) to obtain $(C_n)_{CM} = C_n/m_{CM}$ (Table 1), data which is thus solely relative to the catalytic material. The $(C_n)_{CM}$ values were compared to

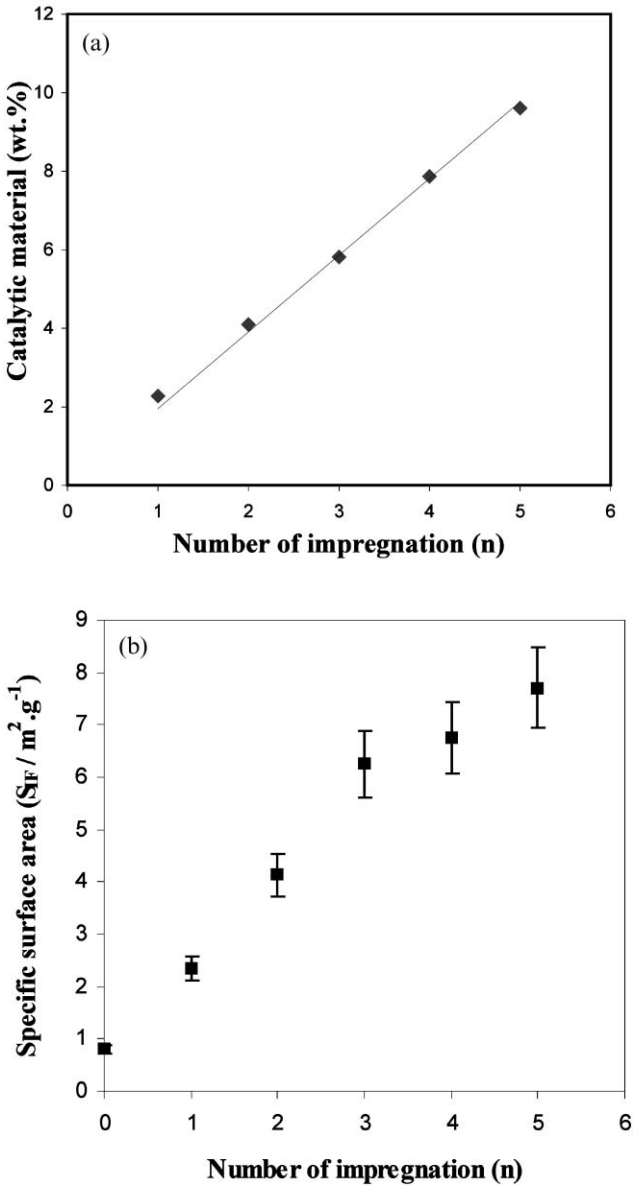

Fig. 4 Weight of impregnated catalytic material (a) and specific surface area of the impregnated foam (b), measured after the 500 °C calcination.

the carbon contents measured in the NP nanocomposite powders ($(C_n)_P$, Table 1) prepared using the corresponding non-milled powders (in powder beds) (Fig. 1) and the same CCVD treatment. The $(C_n)_{CM}$ values are always higher than the $(C_n)_P$ values, notably for samples NF3MP05 and NF3MP20 for which $(C_n)_{CM}$ is at least 3 times higher than the $(C_n)_P$ measured for the corresponding NP05 and NP20 powders, respectively ($(C_n)_{CM}/(C_n)_P$, Table 1). These data clearly show that the CCVD treatment produces more carbon when the catalytic material is attrition-milled and impregnated within the ceramic.

The SEM images of the four NF3MP specimens are reported in Fig. 5, together with an image of the NP05 powder (Fig. 5d). No CNT was detected in sample NF3MP01 (Fig. 5a). However, previous works[22,24] have shown that the selective

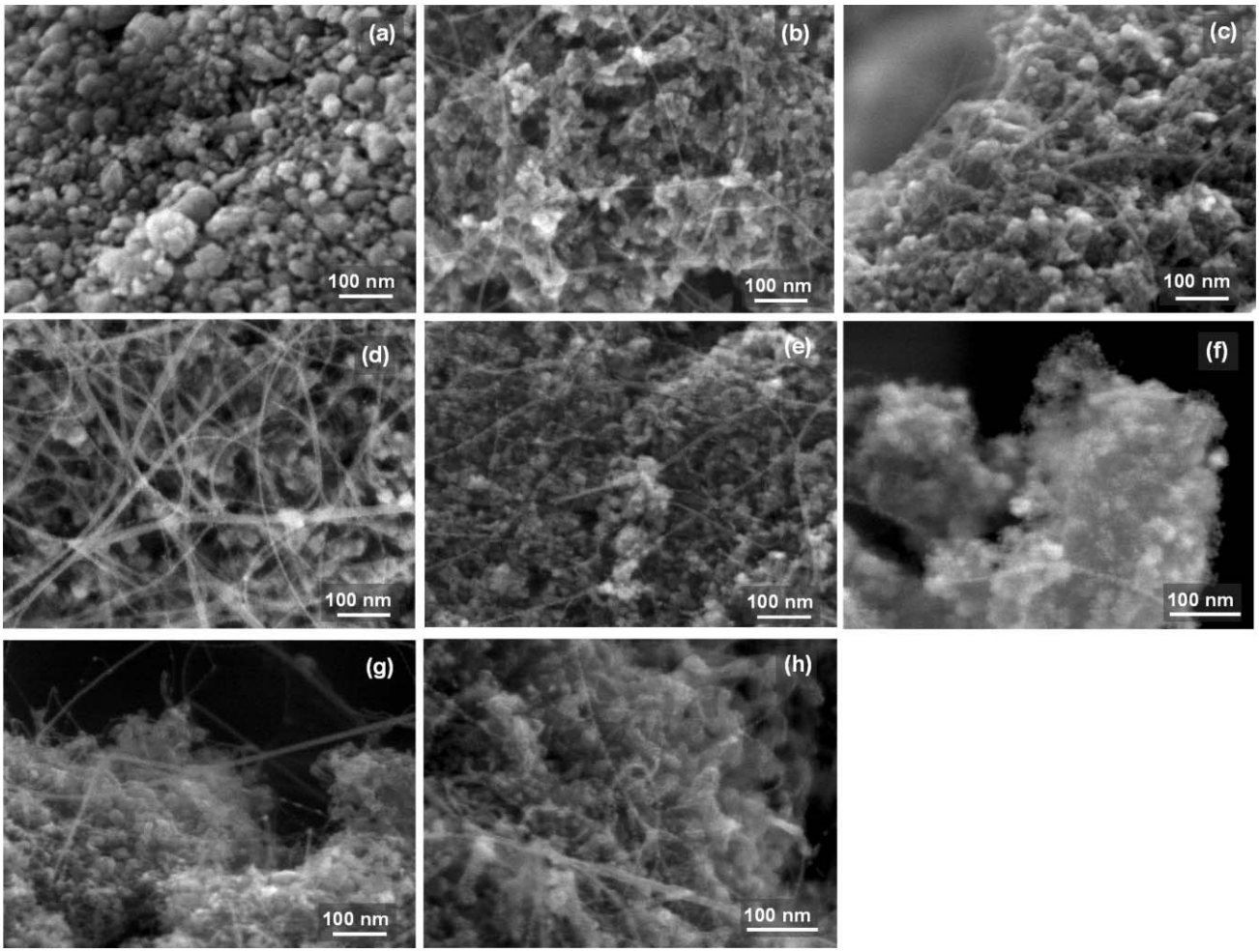

Fig. 5 SEM images of the nanocomposite foams NF3MP01 (a), NF3MP05 (b–c), of the non-milled P05 powder which has been treated in the same conditions (d), of the nanocomposite foams NF3MP10 (e–f) and NF3MP20 (g–h).

reduction of the corresponding NP01 powder bed leads to a great quantity of DWNTs (about 80% of all CNTs). The nature of the deposited carbon thus appears to be very different here since there is slightly more carbon for NF3MP01 ($(C_n)_{CM}$ = 19.9 wt%) than for NP01 ($(C_n)_P$ = 16.1 wt%). For sample NF3MP05 (Fig. 5b, c), some CNTs are observed and it is also revealed that the oxide grains are smaller than for NF3MP01 (Fig. 5a), in agreement with the difference in specific surface area of the starting impregnated foams ($(S_{ss})_{MP}$, Table 1). However, the CNT quantity for NF3MP05 (Fig. 5b–c) is much smaller than for the corresponding NP05 specimen, where there are so many CNTs that they gathered into bundles with diameters in the range 10–20 nm (Fig. 5d). For sample NF3MP10 (Fig. 5e), both CNTs and CNTs bundles are observed, along with some short fibres about 15–20 nm in diameter. Moreover, the SEM image in Fig. 5f shows some carbon species on the foam surface, seemingly made of short and tangled carbon filaments of very small diameter (a few nanometers) which could be CNTs which have not succeeded to grow. For sample NF3MP20 (Fig. 5g–h), many carbon nanofibres, 10–20 nm in diameter and generally short, appear under long and straight CNTs or CNT bundles. In comparison, the corresponding NP20 powder[25] contains both CNTs (mainly MWNTs) and carbon nanofibres, but the latter in a much smaller proportion than for NF3MP20. The nanofibres originate from metal particles that are too large for the formation of CNTs. Indeed, it is known that the critical particle diameter is *ca.* 3 nm.[26,27] The growth of the metal nanoparticles is obviously easier when more of them are formed at the surface of the oxide grains, which is favoured by an increasing metal content (x). Nanoparticles with an intermediate size (6–10 nm) are usually covered by a few graphene sheets (often termed nanocapsules) and are thus inactive for CNT or nanofibre growth. The presence of such nanocapsules can not be ruled out in the present NF3MP samples because they can not be resolved by SEM, but it is worth noting than the involved carbon quantity, if any, is considerably lower than that corresponding to CNTs and nanofibres. The four NF3MP samples were characterised by Raman spectroscopy in order to evaluate the carbon quality, a high intensity ratio ($I_{D/G}$) between the D band (*ca.* 1340 cm^{-1}) and the G band (*ca.* 1574 cm^{-1}) being a signature of a high proportion of undesirable sp^3 carbon including disordered carbon, CNT-wall defects and nanocapsules. For each sample, several spectra were recorded in different areas to evaluate the homogeneity of the material. Representative

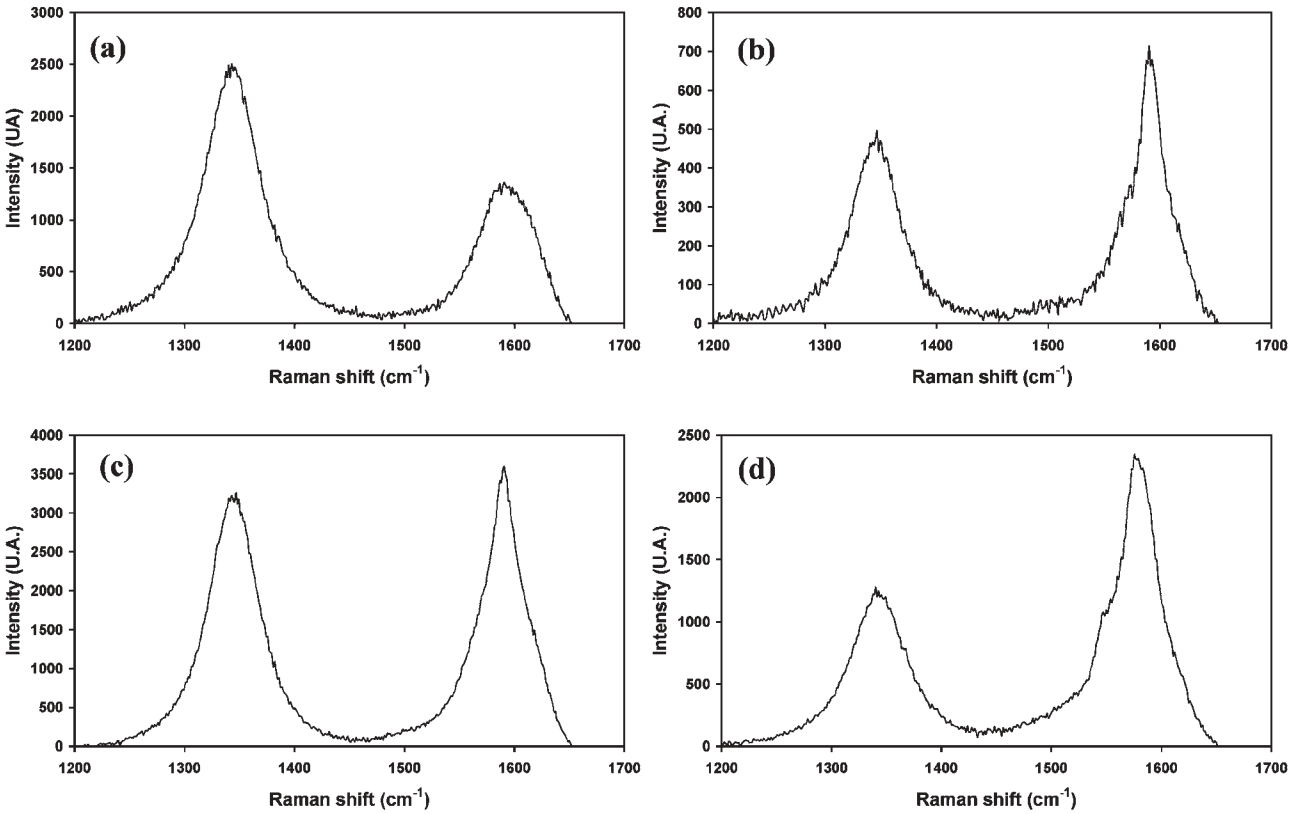

Fig. 6 High-frequency range of the Raman spectra (514.5 nm) showing the D and G bands for the nanocomposite foams NF3MP01 (a), NF3MP05 (b), NF3MP10 (c) and NF3MP20 (d).

spectra are reported in Fig. 6. For sample NF3MP01 (Fig. 6a), $I_{D/G}$ is high (133–164%) and no RBM signal was detected, showing that carbon is probably in the form of disordered carbon or nanocapsules, in good agreement with the SEM observations which failed to reveal any CNT or nanofibre. Spectra of the other samples (NF3MP05, NF3MP10, NF3MP20; Fig. 6b–d) revealed a low homogeneity, $I_{D/G}$ ranging between 30% and 120% depending on the area under examination. Only weak signals were obtained in some areas, probably due to the alumina-based ceramic foam which notably interferes with the CNTs' signal. Moreover, only a few, weak RBM peaks were detected. Thus, the Raman spectra did not allow us to discriminate between the three samples, the carbon qualities being fairly poor. In agreement with the SEM studies, all these samples contain only a small quantity of CNTs. Furthermore, all three samples, particularly NF3MP05, could also contain some disordered carbon and NF3MP10 and NF3MP20 both contain many carbon nanofibres which are probably poorly crystallized.

Both SEM and Raman spectroscopy characterisations showed that, by contrast to what is usually obtained using powder beds of non-milled catalytic materials,[22–25] the carbon is mostly obtained as forms other than CNTs in the present foams. Thus, the catalytic material has become less efficient for the catalytic formation of CNTs with a good selectivity, as a consequence of its milling and its deposition within the ceramic foam. Indeed, the attrition-milling produced smaller oxide grains (<100 nm) and the grain layout by liquid impregnation produced a deposit with a very small porosity (pore diameters < 100 nm). Owing to the very small size of the oxide solid solution grains and the easy diffusion of H_2, the selective reduction became easier, even within the depth of the deposit. The CH_4 supply for the metal nanoparticles formed on the upper side of the deposit is sufficient for CNTs formation, but could become too low for nanoparticles formed deeper in the deposit. For the higher metal contents (NF3MP10 and NF3MP20 samples), the coalescence of the metal particles could be more pronounced because they are not stabilised by a sufficient supply of CH_4, which would favour the formation of nanocapsules or nanofibres. In addition, in order to account for the presence of so many nanofibres, it could be that the metal diffuses by capillarity towards the deposit surface, eventually producing particles that are too large. For the lower metal contents (NF3MP01 and NF3MP05 samples), at least a part of the disordered carbon could have been deposited within the meso- and micro-porosity of the oxide layer, without any role played by the metal nanoparticles.

In the above section, we firstly optimised a process to impregnate commercial ceramic foams with an oxide solid solution powder (catalytic material). Three successive impregnations using a 60 g L^{-1} slurry of attrition-milled powder and absolute ethanol are necessary in order to obtain a homogeneous deposit of catalytic material with a satisfying bonding to the ceramic foam. High carbon contents with respect to the quantity of catalytic material were obtained upon the H_2–CH_4 CCVD treatment. However, most of the carbon was not in the

form of CNTs but mainly in the form of nanofibres and/or disordered carbon, in sharp contrast to what is obtained when using the same catalytic materials in the form of beds of non-milled powders.[22–25] The attrition-milling and deposition onto the walls of the ceramic foam produce a catalytic material with a fine grain size, which favours the formation of metal particles too large for the growth of CNTs. Furthermore, some disordered carbon is also deposited within the micro- and mesopores of the oxide layers. Thus, in the second part of the study, the attrition-milling treatment was omitted from the process in order to obtain a catalytic material deposit with characteristics more resembling those of the corresponding powder beds.

3.3 Foams impregnated with the as-prepared (non-milled) powders

3.3.1 Oxide foams (F*n*P10 specimens). All experiments reported in the present section were carried out using an as-prepared (non-milled) oxide catalytic material of composition $Mg_{0.9}(Co_{0.75}Mo_{0.25})_{0.1}O$ (*i.e.* $x = 0.10$). 60 g L^{-1} slurries were prepared. As in the case of attrition-milled powder, the influence of the number of impregnations was investigated. Up to three impregnations, the adherence of the deposit to the ceramic foam was good, even better than for the samples reported in the previous section, but it decreased for more than three impregnations The quantity of deposited catalytic material (m_{CM}) increases with n (Table 2). For F3P10, the value (m_{CM} = 7.77 wt%) is very close to that obtained for the corresponding F3MP10 (m_{CM} = 7.85 wt%). This shows that the oxide grain size has no significant influence on the quantity of deposited powder *via* the present process. Indeed, the specific surface area of the as-prepared powder (P10) is fairly high (102 m^2 g^{-1}, Table 2) but still significantly lower than that of the corresponding milled powder (MP10, 187 m^2 g^{-1}, Table 1).

3.3.2 Nanocomposite foams (NFnP10 specimens). The carbon content (C_n, Table 2) measured for the NFnP10 nanocomposite foams obtained by CCVD is in the range 3.27–7.57 wt%, increasing with the number of impregnations and thus with the quantity of deposited catalytic material (m_{CM}). The $(C_n)_{CM}$ values (Table 2), relative to the catalytic material are similar (96–120 wt%) for the three NFnP10 specimens, but significantly higher than for both the corresponding NF3MP10 foam (67.6 wt%, Table 1) and the corresponding powder bed (38.6 wt%, Table 2), $(C_n)_{CM}$ is at least 2.5 times higher than the $(C_n)_P$ measured for the corresponding powder-beds, ($(C_n)_{CM}/(C_n)_P$, Table 2), showing that the CCVD treatment produces more carbon when the catalytic material is impregnated within the ceramic.

SEM images of the NF3P10 sample are reported in Fig. 7. The catalytic material layer, which totally covers the foam, is made up of adjacent platelets resulting in a large porosity (Fig. 7a). In the observed areas, all grains are covered by filamentous carbon (Fig. 7b). Interestingly, no carbon nanofibres have been detected. Higher magnification images show that these filaments have the usual characteristics of CNTs or CNT bundles, 1–15 nm in diameter (Fig. 7c–d). The CNT deposit is sufficiently dense and thick to mask the oxide surface. The NF3P10 foam was also studied by Raman spectroscopy. The D and G band positions are respectively 1340 and 1574 cm^{-1} (Fig. 8) The intensity ratio ($I_{D/G}$) varies from 13 to 60% according the area under examination, revealing some degree of heterogeneity, but it is significantly lower than for NF3MP10 (55–95%), which confirms the better overall carbon quality, in agreement with the SEM observations. Moreover, the higher $I_{D/G}$ values were obtained on spectra with low peak intensities, probably corresponding to sample areas where the ceramic is less covered by the catalytic material and thus by the CNTs, or on fractures of the ceramic foam devoid of CNTs. The sharp RBM signals in the low-frequency range (inset in Fig. 8) are also evidence for the good quality of the CNTs, similar to that obtained with powder beds.[22,23] Indeed, the RBM peaks at 208.1, 215.1 and 285.8 cm^{-1} could correspond to isolated or bundled SWNTs with diameters in the range 1.08–1.19 nm, 1.04–1.15 nm and 0.78–0.87 nm, respectively.[28–30]

To conclude this section, it was shown that the NF3P10 sample, prepared by impregnation of the ceramic foam with a non-attrition-milled powder, presents a less compact deposit which better adheres to the commercial ceramic foam. Moreover, after the CCVD treatment, carbon is chiefly in the form of CNTs, their quality seeming close to that obtained with powder beds and their quantity being about 2.5 times higher. Indeed, the unfavourable influence of too small oxide grains and a too small porosity of the oxide deposit that occur when using attrition-milled powders has been avoided and therefore the CH_4 supply to the metallic nanoparticles has

Table 2 Characteristics of the oxide foams prepared using 60 g L^{-1} slurries made with non-milled powders (FnP10 samples) and of the corresponding nanocomposite foams (NFnP10 samples) obtained after the CCVD treatment. All data are reported versus the number of impregnations (n) for specimens with $x = 0.1$ in the starting oxide solid solution $Mg_{(1-x)}(Co_{0.75}Mo_{0.25})_xO$

n		1	2	3
P10	$(S_{ss})_P$ (m^2 g^{-1})	102 ± 3.1	102 ± 3.1	102 ± 3.1
FnP10	m_{CM} (wt%)	2.73 ± 0.62	5.78 ± 0.53	7.85 ± 0.53
NFnP10	C_n (wt%)	3.27 ± 0.33	5.89 ± 0.59	7.57 ± 0.76
	$(C_n)_{CM}$ (wt%)	120 ± 31	102 ± 11	96 ± 8
Foam/powder bed comparison	$(C_n)_{CM}/(C_n)_P$	3.1	2.6	2.5

[a] $(S_{ss})_P$: specific surface area of the non-milled oxide powders. [b] m_{CM}: mass of the corresponding catalytic material (wt%) impregnated in the commercial foam. [c] C_n: carbon content (wt%) in the nanocomposite foam after CCVD treatment, relative to the mass of the nanocomposite foam. [d] $(C_n)_{CM}$: carbon content (wt%) in the nanocomposite foam after CCVD treatment, relative to the mass of catalytic material impregnated in the foam. [e] $(C_n)_{CM}/(C_n)_P$: foam/powder bed comparison with $(C_n)_P$ = 38.6 ± 0.8 wt% (Table 1).

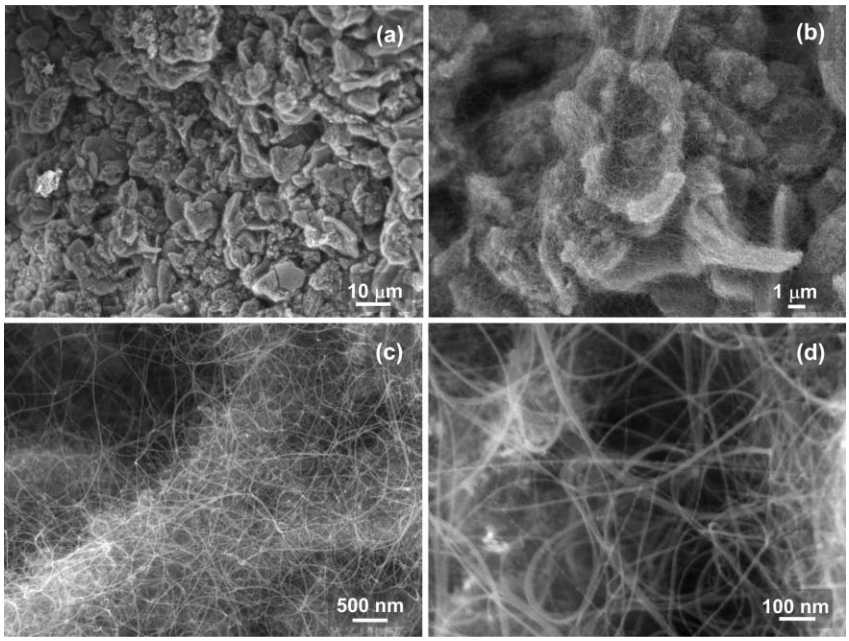

Fig. 7 SEM images of the nanocomposite foam NF3P10 at increasing magnifications showing the deposit of catalytic material (a–b) and the high quantity and good quality of CNTs (b–d).

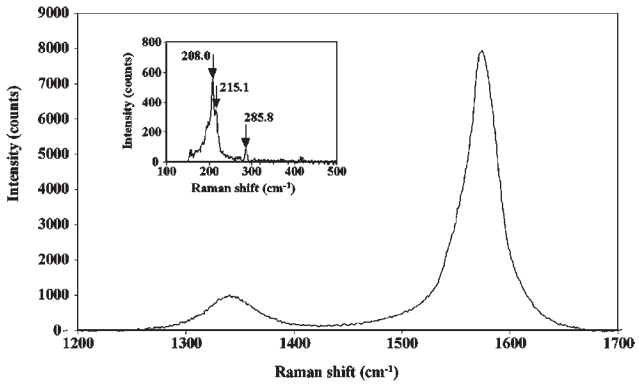

Fig. 8 High-frequency range of the Raman spectrum (514.5 nm) for the NF3P10 nanocomposite foam showing the D and G bands (*ca.* 1340 and 1574 cm^{-1}, respectively) and (inset) the RBM range.

become easier than in both the foams impregnated by attrition-milled powder and the powder bed, leading to a better overall efficiency of the catalytic material with respect to the formation of CNTs.

Many authors have shown that CNTs are interesting as substrates for catalytic nanoparticles.[9–14] Thus, in view of the possible application of the present CNT–foam composite material, a breakdown of the available surface area in the NF3P10 sample has been conducted. Firstly, the ceramic foam gives the material its mechanical resistance and also provides a structure with a widely open porosity at the millimetre scale. It has a low specific surface area (0.8 ± 0.1 m^2 g^{-1}). Secondly, the catalytic material also contributes to the structuration of the pore walls, besides its obvious role in the *in situ* formation of CNTs. It brings a surface area ($(S_{ss})_p \times m_{CM}$, Table 2) equal to *ca.* 8 m^2 to each gram of composite material. Thirdly, the CNTs bring a surface area of *ca.* 15 m^2 to each gram of composite material. Due to the multi-scale structuration of the composite material, any other catalytic material deposited on the CNTs surface would be easily accessible to large gas flow. Studies of the deposition of metallic nanoparticles within the present CNT-composite foams are in progress.

4.0 Conclusions

Consolidated nanocomposite foams, containing a large quantity of CNTs within millimetre-sized pores, were prepared for the first time. The process includes the impregnation of a commercial ceramic foam by a 60 g L^{-1} slurry of a $(Mg_{(1-x)}(Co_{0.75}Mo_{0.25})_xO$ solid solution (x = 0.01, 0.05, 0.1 and 0.2) powder in ethanol. Impregnations in three steps led to deposits, several tens of micrometre thick, with a good coverage of all the commercial-ceramic pore walls but without closing the pores. In the first part of the study, attrition-milled powders with x = 0.01, 0.5, 0.10 and 0.20 were used for the impregnation. The materials were submitted to a CCVD treatment in H_2–CH_4 atmosphere in order to form the CNTs by selective reduction of the solid solution. High carbon contents (with respect to the quantity of catalytic material) were obtained, but most of the carbon was in the form of nanofibres or disordered carbon rather than CNTs, in contrast to what is obtained when using a powder bed of the same catalytic material without any attrition-milling. In the second part of the study, the commercial ceramic foam was impregnated with a powder (x = 0.10) slurry but without attrition-milling, leading to a less compact deposit with a higher adherence to the walls of the ceramic foam. After the CCVD treatment, the carbon is mostly in the form of high-quality CNTs, similar to what is obtained with powder beds, their quantity however being 2.5 times higher. Owing to the large porosity of both the ceramic foam and the catalytic oxide layer, the CH_4 supply to the catalytic metal nanoparticles

formed upon reduction has become much easier than in powder beds, leading to a higher efficiency of the catalytic material. The so-obtained consolidated nanocomposite materials show a multi-scale pore structuration, the very well distributed CNTs offering a surface area of *ca.* 15 m^2 for each gram of composite material. These CNTs are suitable substrates for catalytic nanoparticles which would be very easily accessible to large gas flow.

Acknowledgements

The authors thank Dr T. Chartier and Dr F. Rossignol (SPCTS, UMR CNRS 6638, Limoges, France) for scientific discussions related to the preparation of the ceramic slurries.

References

1 J. T. Richardson, D. Remue and J. K. Hung, *Appl. Catal., A*, 2003, **250**, 319–329.
2 J. T. Richardson, Y. Peng and D. Remue, *Appl. Catal., A*, 2000, **204**, 19–32.
3 C. Agrafiotis and A. Tsetsekou, *J. Eur. Ceram. Soc.*, 2000, **20**, 815–824.
4 A. Sirijaruphan, J. G. Goodwin, Jr., R. W. Rice, D. Wei, K. R. Butcher, G. W. Roberts and J. Spivey, *Appl. Catal., A*, 2005, **281**, 11–18.
5 N. Jarrah, J. G. van Ommen and L. Lefferts, *Catal. Today*, 2003, **79**, 815–824.
6 R. S. Ruoff and D. C. Lorents, *Carbon*, 1995, **33**, 925–930.
7 T. W. Ebbesen, H. J. Lezc, H. Hiura, J. W. Bennet, H. F. Ghaemi and T. Thio, *Nature*, 1996, **382**, 54–56.
8 A. Peigney, Ch. Laurent, E. Flahaut, R. R. Bacsa and A. Rousset, *Carbon*, 2001, **139**, 507–514.
9 W. Li, C. Liang, J. Qiu, W. Zhou, H. Han, Z. Wei, G. Sun and Q. Xin, *Carbon*, 2002, **40**, 787–803.
10 J. Zhu, M. Yudasaka and S. Iijima, *Chem. Phys. Lett*, 2003, **380**, 496–502.
11 J. M. Planeix, N. Coustel, B. Coq, V. Brotons, P. S. Kumbhar, R. Dutartre, P. Geneste, P. Bernier and P. M. Ajayan, *J. Am. Chem. Soc.*, 1994, **116**, 7935–7936.
12 P. Serp, M. Corrias and P. Kalck, *Appl. Catal., A*, 2003, **253**, 337–358.
13 V. Lordi, N. Yao and J. Wei, *Chem. Mater.*, 2001, **13**, 733–737.
14 M. J. Ledoux, R. Vieira, C. Pham-Huu and N. Keller, *J. Catal.*, 2003, **216**, 333–342.
15 A. Peigney, Ch. Laurent, F. Dobigeon and A. Rousset, *J. Mater. Res.*, 1997, **12**, 613–615.
16 E. Flahaut, A. Govindaraj, A. Peigney, Ch. Laurent and A. Rousset, *Chem. Phys. Lett.*, 1999, **300**, 236–242.
17 E. Flahaut, A. Peigney, Ch. Laurent and A. Rousset, *J. Mater. Chem.*, 2000, **10**, 249–252.
18 S. Rul, Ch. Laurent, A. Peigney and A. Rousset, *J. Eur. Ceram. Soc.*, 2003, **23**, 1233–1241.
19 S. Rul, A. Peigney, W. S. Bacsa and Ch. Laurent, to be published.
20 K. C. Patil, *Bull. Mater. Sci.*, 1993, **16**, 533–541.
21 J. Kingsley and L. R. Pederson, *Mater. Res. Soc. Symp. Proc.*, 1993, **296**, 361–366.
22 E. Flahaut, A. Peigney, W. S. Bacsa, R. R. Bacsa and Ch. Laurent, *J. Mater. Chem.*, 2004, **14**, 646–653.
23 E. Flahaut, Ch. Laurent and A. Peigney, *Carbon*, 2005, **43**, 375–383.
24 E. Flahaut, R. Bacsa, A. Peigney and Ch. Laurent, *Chem. Commun.*, 2003, 1442–1443.
25 E. Flahaut, L. Frin, A. Peigney and Ch. Laurent, to be published.
26 J. H. Hafner, M. J. Bronikowski, B. K. Azamian, P. Nikolaev, A. G. Rinzler, D. T. Colbert, K. A. Smith and R. E. Smalley, *Chem. Phys. Lett.*, 1998, **296**, 195–202.
27 A. Peigney, P. Coquay, E. Flahaut, R. E. Vandenberghe, E. De Grave and Ch. Laurent, *J. Phys. Chem. B*, 2001, **105**, 9699–710.
28 S. Bandow, S. Asaka, Y. Saito, A. M. Rao, L. Grigorian, E. Richter and P. C. Ecklund, *Phys. Rev. Lett.*, 1998, **80**, 3779–1998.
29 L. Alvarez, A. Righi, T. Guillard, S. Rols, E. Anglaret, D. Laplaze and J.-L. Sauvajol, *Chem. Phys. Lett.*, 2000, **316**, 186–190.
30 A. Jorio, M. A. Pimenta, A. G. Souza Filho, R. Saito, G. Dresselhaus and M. S. Dresselhaus, *New J. Phys.*, 2003, **5**, 139.1–139.17.